Magnetic field effect on the cooling of a low-Pr fluid in a vertical cylinder

I. E. Sarris, A. I. Iatridis, C. D. Dritselis, and N. S. Vlachos

Citation: Physics of Fluids (1994-present) **22**, 017101 (2010); doi: 10.1063/1.3291074
View online: http://dx.doi.org/10.1063/1.3291074
View Table of Contents: http://scitation.aip.org/content/aip/journal/pof2/22/1?ver=pdfcov
Published by the AIP Publishing

Magnetic field effect on the cooling of a low-Pr fluid in a vertical cylinder

I. E. Sarris,[a] A. I. Iatridis,[b] C. D. Dritselis,[c] and N. S. Vlachos[d]
Department of Mechanical Engineering, Laboratory of Fluid Mechanics and Turbomachines, University of Thessaly, Volos 38334, Greece

(Received 4 March 2009; accepted 12 December 2009; published online 11 January 2010)

Results of direct numerical simulations are presented for the transient and turbulent natural convection cooling of an initially isothermal quiescent liquid metal placed in a vertical cylinder in the presence of a vertical magnetic field. The electrically conductive low-Prandtl number fluid is put to motion when the cylindrical wall is suddenly cooled to a uniform lower temperature. For this particular cooling process, the flow is characterized by three sequential almost discrete stages: (a) development of momentum and thermal boundary layers along the cylindrical cold wall, (b) intrusion of the cooled fluid into the main fluid body, and (c) flow and thermal stratification. The selected Rayleigh numbers in the present study are high enough so that turbulent convection is established. The numerical results show that the magnetic field has no observable effect at the initial stage of the vertical boundary layer development and conduction heat transfer is favored during the intrusion stage. An interesting effect of the magnetic field during the stratification stage is the deceleration of the cooling process for low Rayleigh numbers and its acceleration for high ones. This dependence of the magnetic field effect on the Rayleigh number was found to be related to the cold vortices emanating from the vertical boundary layer. In contrast with the hydrodynamic cooling, the magnetic field was also found to accelerate the cooling near the bottom of the cylinder. © *2010 American Institute of Physics*. [doi:10.1063/1.3291074]

I. INTRODUCTION

A significant variety of natural flows and industrial applications are subjected to thermal convection driven by horizontal temperature gradients. Some of these flows consider heat transfer horizontally in cylindrical water tanks (for example, Papanicolaou and Belessiotis),[1] stratification in thermosyphon or air systems under electromagnetic and buoyant forces (Lee and Hyun),[2] and crystal growth (for example, Davoust *et al.*)[3] where the effect of magnetic fields was taken into account. In all these applications, the resulting flow is highly unsteady and the fluid responds fast to temperature changes.

In contrast with other natural convection configurations (for example, Rayleigh–Bérnard convection[4] or laterally heated enclosures),[5] the present cooling process is not statistically stationary, except at the final motionless state. The entire process, starting from a homogeneous, hot and quiescent fluid, is characterized by three stages: (a) development of flow and thermal boundary layers on the cylindrical wall, (b) thermal intrusion of the cold fluid into the bulk from the bottom corner of the cylinder, and (c) flow and thermal stratification. All these stages happen in series resulting finally to a fluid at rest having a uniform lower temperature, as determined by the imposed thermal boundary condition on the vertical wall. A discussion of previous work on this subject can be found in Lin and Armfield[6] and also in the review article of Hyun.[7]

Past research considered mainly liquids and gases with Prandtl numbers much higher than those of liquid metals. The numerous studies of natural convection cooling of fluids with Prandtl numbers higher than unity can be explained by the practical interest on the cool-down process due to flooding of the reactor cavity of nuclear power plants in case of accident.[8] An exception seems to be the work of Hyun[9] where the effect of the Prandtl number was studied and its significance in the heating-up was assessed. The scaling laws of the cooling in a vertical cylinder filled with a fluid of Prandtl number less than unity was also studied by Lin and Armfield.[10] They provided arguments about the importance of three-dimensional simulations for natural convection cooling. In particular, they indicated that no three-dimensional patterns are expected during the stage of boundary layer development because of different time scales, and also during the stratification stage because the local Rayleigh number is steadily reduced. Finally, Lin *et al.*[11] recently studied the low-Prandtl number regime of the cooling process in a rectangular container using numerical and scaling techniques.

It appears that research has been conducted mainly for laminar or transitional flows with relative small or moderate Rayleigh numbers where the demand in computer power and memory is not very high. Moreover, studies at very high Rayleigh numbers ($\geqslant 10^{12}$) and high turbulence intensities have been carried out with the use of eddy-viscosity subgrid models in large-eddy simulations or simpler models like the $k-\epsilon$. Such turbulence models have been used already in various magnetohydrodynamic applications, for example, for the study of homogeneous turbulence with large-eddy simulations by Knaepen and Moin[12] and for various magnetohydrodynamic flow configurations by Kenjereš and Hanjalić.[13]

[a]Electronic mail: sarris@mie.uth.gr.
[b]Electronic mail: iatrid@mie.uth.gr.
[c]Electronic mail: dritseli@mie.uth.gr.
[d]Electronic mail: vlachos@mie.uth.gr.

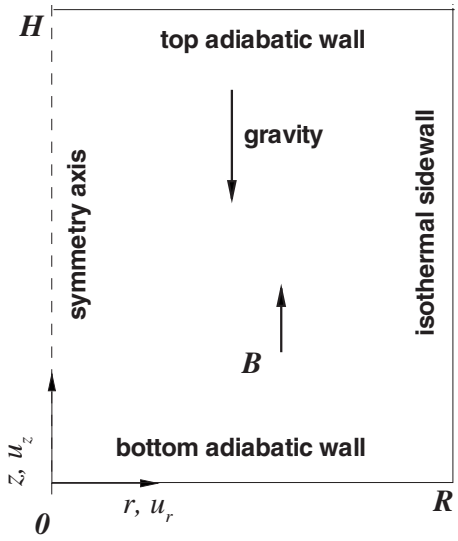

FIG. 1. Flow geometry and boundary conditions.

For the flow in an axisymmetric container, direct numerical simulations can be found even at very high Rayleigh numbers, while recently three-dimensional direct numerical simulations for $\mathrm{Ra}=2\times10^{11}$ have been presented by Verzicco and Camussi.[4] For all these cases, the working fluid considered has Prandtl numbers close to unity. However, for thermal buoyant flows, the theory of turbulence connects the smallest eddy size of the flow with the values of the Rayleigh and Prandtl numbers.[14] This means that for direct numerical simulations at very large Rayleigh number fine grids are required.

In the present study, the effect of a constant vertical magnetic field on the cooling process of a liquid metal confined in a vertical cylindrical container is considered. To the authors best knowledge this is the first attempt to study the magnetic field effect on the cooling of liquid metals in this configuration. The use of a direct numerical simulation method for the calculation of the axisymmetric turbulent flow ensures maximum accuracy. The results presented, except of their theoretical value, have also practical use. The application that motivated this study is the cooling of hot liquid metals in heat exchanging devices of future fusion reactors. In the present configuration, heat is transferred from the hot fluid to the colder container walls and, thus, the fluid is getting colder.

II. PROBLEM DEFINITION

A. Governing equations

The magnetohydrodynamic problem considered here is the natural convection cooling of a low-Prandtl number fluid placed in a vertical cylindrical container of height H, radius R, and a fixed aspect ratio $R/H=1$, as shown in Fig. 1. The upper and lower horizontal boundaries are adiabatic walls, while all rigid boundaries are electrically insulated. Initially the fluid is at rest and at uniform temperature T_0. Suddenly at $t=0$, the cylindrical wall is cooled to a constant temperature $T_w<T_0$. A vertical magnetic field of magnitude B_0 is also imposed externally interacting with the natural convection cooling which proceeds for $t>0$.

The governing equations of the present axisymmetric thermally driven flow are the mass continuity equation, the incompressible Navier–Stokes equations with the usual Boussinesq approximation for the buoyancy term, and the energy conservation equation. The effect of the constant vertical (axial) magnetic field on the fluid is added through the Lorentz force to the momentum equation. For the calculation of this magnetic damping term, the low magnetic Reynolds number approximation was used.[15] In this approximation, the induced magnetic field is considered very weak when compared with the external magnetic field B_0. This is true for low magnetic Reynolds numbers as those of liquid-metal flows used in laboratory scale experiments. A useful discussion for the validity limits of this approximation in natural convection flows can be found in Sarris *et al.*[16]

The magnetohydrodynamic equations were made dimensionless using as characteristic quantities, the height of the cylinder H, the temperature difference $\Delta T=T_0-T_w$, the amplitude of the external magnetic field B_0, and the free fall velocity $u_0=(g\beta H\Delta T)^{1/2}$, where g is the gravity acceleration, and β the volumetric thermal expansion coefficient of the fluid. Since an axial magnetic field is considered in the present simulations, the flow can still be assumed as axisymmetric because the Lorentz force is independent of the azimuthal angle. This axisymmetry has been demonstrated in the case of a cylindrical container with an applied sinusoidal temperature on its upper lid by Kakarantzas *et al.*[17] However, this is not true for the case of homogeneous turbulence[18] or for an inclined or horizontal magnetic field, the action of which depends strongly on the azimuthal angle, as shown by Kakarantzas *et al.*[19]

The nondimensional governing equations in cylindrical coordinates read as follows:

$$\frac{1}{r}\frac{\partial(ru_r)}{\partial r}+\frac{\partial u_z}{\partial z}=0, \tag{1}$$

$$\frac{\partial u_r}{\partial t}+\frac{1}{r}\frac{\partial(ru_ru_r)}{\partial r}+\frac{\partial(u_zu_r)}{\partial z}=-\frac{\partial p}{\partial r}+\left(\frac{\mathrm{Pr}}{\mathrm{Ra}}\right)^{1/2}\left\{\frac{\partial}{\partial r}\left[\frac{1}{r}\frac{\partial(ru_r)}{\partial r}\right]+\frac{\partial^2u_r}{\partial z^2}\right\}-\mathrm{Ha}^2\left(\frac{\mathrm{Pr}}{\mathrm{Ra}}\right)^{1/2}u_r, \tag{2}$$

$$\frac{\partial u_z}{\partial t}+\frac{1}{r}\frac{\partial(ru_ru_z)}{\partial r}+\frac{\partial(u_zu_z)}{\partial z}=-\frac{\partial p}{\partial z}+\left(\frac{\mathrm{Pr}}{\mathrm{Ra}}\right)^{1/2}\left\{\frac{1}{r}\frac{\partial}{\partial r}\left(r\frac{\partial u_z}{\partial r}\right)+\frac{\partial^2u_z}{\partial z^2}\right\}+\theta, \tag{3}$$

$$\frac{\partial\theta}{\partial t}+\frac{1}{r}\frac{\partial(ru_r\theta)}{\partial r}+\frac{\partial(u_z\theta)}{\partial z}=\frac{1}{(\mathrm{Ra\,Pr})^{1/2}}\left[\frac{1}{r}\frac{\partial}{\partial r}\left(r\frac{\partial\theta}{\partial r}\right)+\frac{\partial^2\theta}{\partial z^2}\right], \tag{4}$$

where p is the dimensionless pressure, u_r and u_z are the dimensionless radial and axial velocity components, and r and z are the dimensionless radial and axial coordinates, respectively. The temperature T is made dimensionless by using the quantity $\theta=(T-T_0)/(T_0-T_w)$. The effect of viscous dissipation and Joule heating on the present flow is neglected. These simplifications are almost universal for all magnetohydrodynamic natural convection flows. A comprehensive justification for the latter can be found in Gelfgat and Bar-Yoseph.[20]

The present flow depends on three dimensionless parameters: the Rayleigh number (Ra), the Prandtl number (Pr), and the Hartmann number (Ha) defined as

$$\mathrm{Ra}=\frac{g\beta H^3\Delta T}{\nu\alpha},\quad \mathrm{Pr}=\frac{\nu}{\alpha},\quad \mathrm{Ha}=B_0H\sqrt{\frac{\sigma}{\rho\nu}}, \tag{5}$$

where ν is the kinematic viscosity, α the thermal diffusivity, σ the electrical conductivity, and ρ the density of the fluid.

The initial and boundary conditions are the following:

$$\text{for } t<0:\quad u_r=u_z=\theta=0,$$

$$\text{for } t\geq 0:\quad u_r=u_z=0,\quad \frac{\partial\theta}{\partial z}=0 \text{ for } z=0 \text{ and } 1,$$

$$u_r=0,\quad \frac{\partial u_z}{\partial r}=\frac{\partial\theta}{\partial r}=0 \quad \text{for} \quad r=0,$$

$$u_r=u_z=0,\quad \theta=-1, \text{ for } r=1.$$

In order to study the heat transfer characteristics of the flow, an instantaneous Nusselt number which is averaged along the isothermal cylindrical wall is calculated from

$$\mathrm{Nu}=\frac{1}{H}\int_0^H\left(-\frac{\partial\theta}{\partial r}\right)_{r=1}dz. \tag{6}$$

A streamfunction Ψ is calculated from the velocity fields via $u_r=\partial\Psi/\partial z$. It is also convenient to define a measure for the average bulk temperature, T_a, during the transient cooling as suggested in Ref. 10. The dimensionless average temperature in each time step is defined as $\theta_\alpha(t)=(T_a-T_0)/(T_0-T_w)$. Initially, at $t=0$ the average bulk temperature is equal to the temperature T_0 of the resting fluid and, thus, $\theta_\alpha(0)=0$.

B. Numerical method and simulation details

The governing equations (1)–(4) were discretized in a staggered nonuniform mesh with second-order accurate finite differencing, as suggested by Verzicco and Orlandi.[21] The final system of algebraic equations was solved with a fractional step method. The diffusion terms were advanced in time with a Crank–Nicolson method, while the nonlinear terms, the buoyancy term and the Lorentz force with an economic third-order Runge–Kutta method. The present numerical method requires the solution of a Poisson equation for the pseudopressure (see Refs. 21 and 22 for more details), which was discretized with central differencing. The solution of the resulting tridiagonal matrix was obtained with the FISHPACK library.[23]

Several direct numerical simulations were performed by using a liquid metal with Pr=0.02, Rayleigh numbers in the range of $1\times10^7\leq\mathrm{Ra}\leq2\times10^9$ and Hartmann numbers between 0 and 300. When a direct simulation is performed, the size of the computational cells must be of the same order (or smaller) compared to the size of the smallest eddies of the flow (Kolmogorov length, η). Moreover, the viscous boundary layers on the solid boundaries must also be resolved efficiently. The latter implies that inside the velocity boundary layer of thickness δ_u, a minimum number of computational cells must be distributed, a condition that is in general stricter than the Kolmogorov length scale. The temperature field has also analogous discretization demands imposed by the Batchelor characteristic length scale, η_T, and the thickness of the thermal boundary layer, δ_θ. The above constrains must be fulfilled simultaneously and, thus, the main focus is to satisfy the more restrictive. In practice, constrains for the quantities δ and η are of different importance in different regions of the flow, the former near the walls and the latter in the main fluid body.

The external magnetic field B_0 in the presence of the solid boundaries adds extra constrains because it results in the formation of magnetic boundary layers (Hartmann and sidewall diffusion layers, see Alboussière and Lingwood).[24] The Hartmann layers are formed along walls that are normal to the magnetic field and their thickness is proportional to Ha^{-1}, while the sidewall diffusion layers are formed on the parallel walls with thickness proportional to $\mathrm{Ha}^{-1/2}$.[15] When the Hartmann number is high enough, the magnetic boundary layer constrains on grid size are more restrictive than those of the momentum and thermal boundary layers, and it is very difficult to satisfy them, especially in three-dimensional direct numerical simulations.

For the reasons described above, a nonuniform grid based on hyperbolic tangent distribution functions was used for both the axial and radial directions in order to cover the boundary layers on the top and bottom horizontal walls, on the cylindrical wall, and in the region near the symmetry axis. The latter is due to observations based on numerical experiments by Lin and Armfield[6,25] for the fluid cooling paths which will be discussed below. For a working fluid with $\mathrm{Pr}\leq1$ it is known that $\eta\leq\eta_T$, and according to Grötzbach,[26] a reasonable estimation of the Kolmogorov scale is $\eta/H\sim\pi(\mathrm{Pr}^2/\mathrm{RaNu})^{1/4}$. This analysis, in combination with a suitable relationship for the Nusselt number, can give an estimate for η. Moreover, it is known that the Kolmogorov theory gives the order of magnitude and not the exact value of η that is needed to be resolved (see Moin and Mahesh).[27]

For typical magnetohydrodynamic natural convection flows of liquid metals, the Nusselt number is an exponential function of the Ra and Ha numbers (see, for example, Aurnou and Olson).[28] The difference in the present flow is that in the first stage of development of the thermal boundary

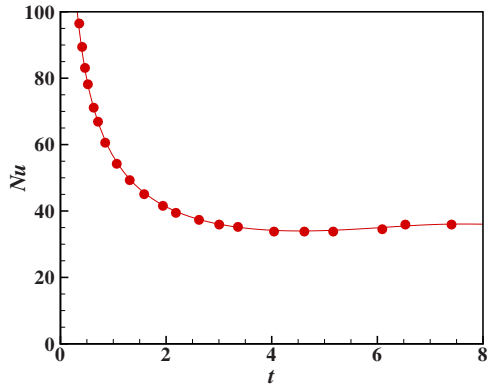

FIG. 2. (Color online) Comparison of the present model (solid line) with the results of Lin and Armfield (Ref. 10) (points) for the case $\mathrm{Ra}=10^8$, $\mathrm{Pr}=0.1$, and $R/H=1$.

layer on the cylindrical wall, a very fast change in the Nusselt number, as shown in Fig. 2, is happening which depends only on the Rayleigh number and it is completely independent of Ha. After the initial steep change in the Nusselt number, its value is stabilized for $t>4$. The thermal boundary layer is still present during the intrusion stage and its size is reduced only during the stratification stage. This can be seen in Fig. 3, where the time evolution of the streamfunction and temperature fields of the hydrodynamic and magnetohydrodynamic cases for $\mathrm{Ra}=10^9$ are compared.

For the present hydrodynamic natural convection flow, the numerical simulations and scale analysis of Lin and Armfield[6] have shown that the relationship $\mathrm{Nu}\sim\mathrm{Ra}^{1/4}t^{-1/2}$ is valid during the development stage of the vertical boundary layer. For the analysis conducted here, this relation was used for $t=6$ and, in combination with the other flow parameters, gives a value $\eta/H\simeq 0.001$, for the most convective case of $\mathrm{Ra}=2\times10^9$ studied. This specific value of time was selected because it is close to the time where the development of the thermal boundary layer is completed; the fluid ascends along

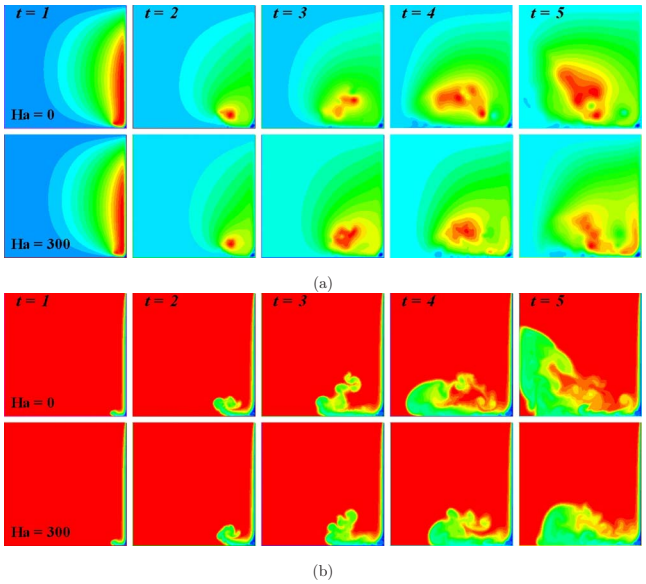

FIG. 3. (Color online) Distribution of streamfunction (a) and temperature (b) for $\mathrm{Pr}=0.02$, $\mathrm{Ra}=10^9$ at $1\le t\le 5$: Ha=0 (upper), 300 (lower).

TABLE I. Parameters and mesh sizes of the simulations.

Ra	$\Delta r=\Delta z$	δ_u	$nr\times nz$
1×10^7	0.0083	0.0033	128×128
1×10^8	0.0053	0.0016	196×196
5×10^8	0.0035	0.0012	320×320
1×10^9	0.0025	0.0008	384×384
2×10^9	0.00125	0.0004	512×512

the symmetry axis of the container and continues to move along the upper horizontal wall, while the intrusion stage is starting along the bottom wall.

The thickness of the momentum and thermal boundary layers are related by $\delta_u\sim\delta_\theta\,\mathrm{Pr}$, and δ_θ can be calculated from the relation $\delta_\theta/H\sim 1/2\,\mathrm{Nu}$. For the Hartmann numbers used here, the velocity boundary layer is thinner (e.g., $\delta_u/H\simeq 0.0004$ for $\mathrm{Ra}=2\times10^9$) than the side diffusion layer on the vertical wall, so there is no stricter constrain in the radial direction. However, we must maintain the same grid arrangement in the vertical direction due to the thinner Hartmann layers. Only for the less turbulent case of $\mathrm{Ra}=10^7$ and Ha=300, the velocity boundary layer is of similar thickness with the Hartmann layer. This estimate of δ_u was used *a priori* for the grid distribution within the boundary layers with up to six grid points inside them, where the first point was placed at a distance of $\delta_u/8$ from the wall.

Taking into account all the above restrictions, the mesh sizes nr and nz in the radial and the axial direction, respectively, of each case of Rayleigh number selected are presented in Table I, where Δr and Δz are the maximum distances of the mesh in the respective directions. A time step in the range $\Delta t=0.5$ to $5.\times10^{-5}$, was used depending on the case. The adequacy of the grid size was assessed for some cases by using grids of double size than those of Table I without significant differences in the Nusselt number, which is the most sensitive quantity to the spatial discretization according to Grötzbach.[26] Furthermore, the results of the present numerical method are compared against those of Lin and Armfield[10] for the hydrodynamic case of $\mathrm{Ra}=10^8$, $\mathrm{Pr}=0.1$, and $H/R=1$ using only for this comparison their own dimensionless equations which are slightly different than those of the present study as will be discussed in the next section. The comparison of the Nusselt numbers already presented in Fig. 2 shows an excellent agreement.

Finally, it should be noted that the axisymmetry of the flow may not apply for every case studied here. Therefore, some of the results may possibly be affected by the assumed axisymmetry and by neglecting the three-dimensional effects. This may be the case when the flow becomes fully turbulent at some stages of the simulations, mostly for the hydrodynamic cases or at low Hartmann numbers.

III. RESULTS AND DISCUSSION

As already mentioned, the cooling of liquids in containers due to horizontal temperature gradients is characterized by three almost discrete stages. The first and shorter stage concerns the formation and development of the momentum

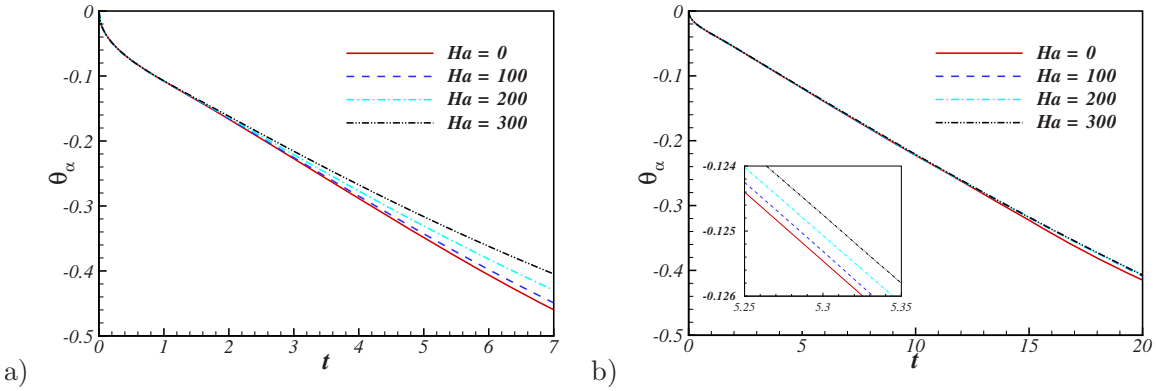

FIG. 4. (Color online) Time variation of the average fluid temperature in the initial cooling stage at different Ha: (a) Ra=10^7 and (b) Ra=10^9.

and thermal boundary layers along the cylindrical wall of the container. Then cold fluid intrudes into the fluid bulk from the corner of the adiabatic bottom wall reaching the center of the container and the final stage of stratification is then starting. The duration of the final stage, like in all other stages, depends on the value of the Rayleigh number according to Lin and Armfield.[6] The asymptotic behavior of the stratification stage for liquids of $\mathrm{Pr} \geq 1$ is discussed in the recent work of Lin and Armfield.[29] The results presented below are focused on the effect of the magnetic field on the natural convection cooling for low-Prandtl number fluids and on the assessment of the effect of Lorentz force in each particular stage of the cooling process.

A. Boundary layer development

From the scale analysis of Lin and Armfield[25] it is known that the boundary layer on the vertical wall becomes fully developed at the dimensionless time $t \sim 1$, having a velocity magnitude $u_z \sim 1$ and thickness $\delta_\theta \sim \mathrm{Ra}^{-1/4}$. It should be noted that in their work, the velocity is made nondimensional by using the characteristic quantity $u_0 = \alpha\, \mathrm{Ra}^{1/2}/H$, which differs from the present nondimensionalization only in the Prandtl number. Despite this, the scaling arguments of the present flow are the same as in Refs. 10 and 25 because only one Prandtl number is studied here. All the magnetohydrodynamic cases simulated show that there is no significant effect of the magnetic field on the flow during the initial stage of the boundary layer development (i.e., for $t < 2$), at least for the range of Hartmann numbers $\mathrm{Ha} \leq 300$ considered here.

A visual proof for the weak effect of the magnetic field during the initial development of the boundary layer is presented by both the streamfunction and temperature fields of Fig. 3 at time $t=1$. No magnetic damping of the fluid motion is expected during this period, because the Lorentz force is proportional to the radial fluid velocity only and no direct interaction exists between the vertical velocity and the parallel magnetic field. The relatively low radial fluid velocities in the boundary layer during the initial stage of the cooling do not permit the development of large Lorentz forces. Moreover, the cylindrical wall is parallel to the magnetic field and, thus, there is no Hartmann layer created on it, which would resist the fluid motion stronger than the side-wall diffusion layers. As a consequence of the weak effect of the magnetic field during the stage of boundary layer development, the average temperature of the fluid (θ_α) shown in Fig. 4 is almost similar for $t<2$ and $t<3$ in the cases Ra $=10^7$ and Ra$=10^9$, respectively, for all magnetic fields studied. The effect of the magnetic field is stronger in the next stage of fluid intrusion, as indicated by the same Fig. 4 for $t>2$ at Ra$=10^7$.

In particular, for the case of Ra$=10^9$ and for time $t=3$, the effect of the magnetic field on the temperature in the bulk of the fluid becomes significant, as shown in Fig. 3, but the region of the vertical boundary layer is not much affected as indicated by the isotherms close to the cylindrical boundary. At this instant, like in all the duration of cooling, no destabilization of the boundary layer was observed. In the magnetohydrodynamic cases studied here, the effect of the magnetic field is to suppress further any possible destabilization because it damps all radial motions inside the boundary layer.

Lin and Armfield[6] demonstrated that the thickness of the thermal boundary layer grows after the initiation of cooling, it reaches a maximum value, δ_θ, at height $z=0.5$ and time $t=1.5$ and then it drops slightly toward steady state. The thickness of the thermal boundary layer at this particular time and position is shown in Fig. 5 for all the cases of Ra and Ha studied. As it is expected from the previous findings, the effect of the magnetic field during boundary layer formation is negligible. This effect is particularly negligible in the cases of high Rayleigh numbers, and only in the case of Ra$=10^7$ are some differences in the thickness of the thermal boundary layer observable. It should be noted that the thickness of the thermal boundary layer in the present results is similar to the findings of Lin and Armfield[10] and, as shown in Fig. 5, it scales linearly with $\mathrm{Ra}^{-1/4}$. These results for the maximum thickness of the thermal boundary layer, and consequently for the thickness of the velocity boundary layer ($\delta_u = \mathrm{Pr}\ \delta_\theta$), are also in agreement with the thickness estimation predicted by the scale analysis which was presented in Sec. II B and was used to select the appropriate mesh distribution shown in Table I. It appears that the momentum and thermal boundary layers are fully resolved by the selected grids.

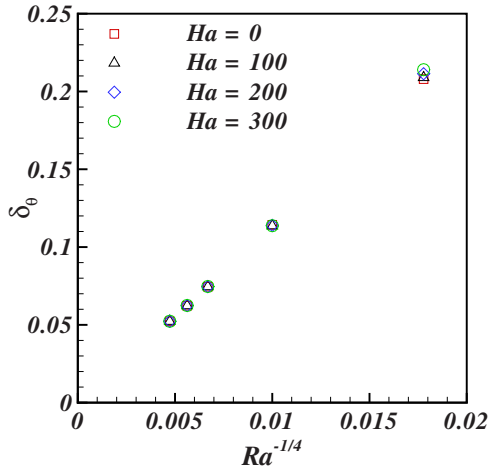

FIG. 5. (Color online) Thickness of the vertical thermal boundary layer at height $z=0.5$ and $t=1.5$.

B. Intrusion stage

The intrusion stage follows the development of the boundary layer on the vertical wall. This stage is characterized by the injection of cold fluid from the boundary layer to the fluid bulk along the horizontal bottom wall. The sequence of the flow evolution at the intrusion stage is well illustrated by the streamfunction and temperature distributions of Fig. 3 at time $t>2$. When the cold fluid reaches the axis of the cylinder this stage is completed. Then, the fluid forms a plume near the axis that ascends toward the upper horizontal wall.

It should be noted that in the older work of Lin and Armfield[6] the intrusion stage was handled separately from the stratification stage, while in their newer work[10,11] a unified analysis is used. The present results indicate that this is an important stage for the cooling process and can be used to explain the mechanism of the damping introduced by the magnetic field. The effect of the magnetic field during the intrusion stage is to produce a significant delay of the cooling, as demonstrated in Fig. 3. The intrusion is characterized primarily by the transfer of axial momentum from the vertical boundary layer to the radial direction. As a consequence of the increase in the radial momentum, the Lorentz force becomes significant. Thus, momentum is transferred slowly to the radial direction and consequently the damping of the magnetic field increases with time. For $t=5$ and Ha=0, the low-temperature fluid from the cylindrical wall reached the symmetry axis near the bottom wall and started to follow a rising course into the bulk along the axis. In contrast, for Ha=300, the thermal intrusion along the horizontal bottom wall is significantly delayed and the rising flow is slower than for Ha=0. The rising flow near the symmetry axis is the reason that a finer grid has been used in this region.

The delay of cold fluid intrusion due to the magnetic field is in principle little affected by the Rayleigh number, as indicated by the results of Fig. 4. The stronger the magnetic field, the hotter remains the fluid in average. This connects the damping action of the magnetic field with the promotion of conduction against convection heat transfer and corresponds to the usual magnetic effect for most of the magnetohydrodynamic natural convection flows. However, the ac-

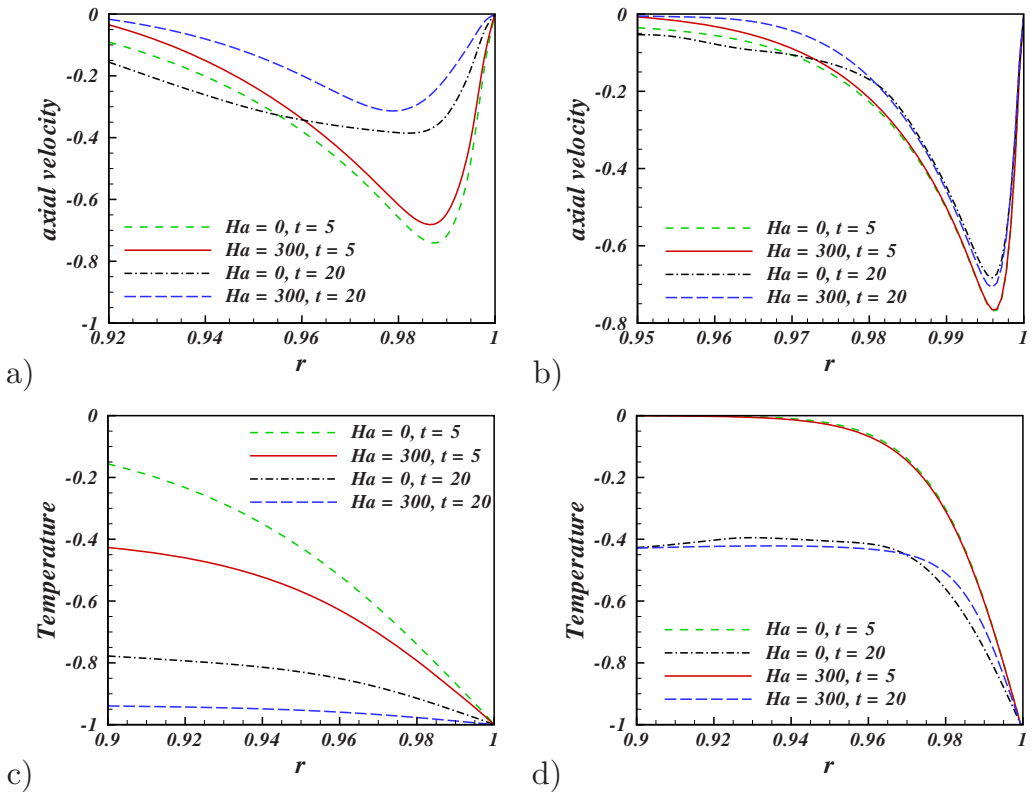

FIG. 6. (Color online) Distribution of the axial velocity (upper) and temperature (lower) at height $z=0.5$, times $t=5$ and 20, and different Hartmann numbers: Ra=10^7 (left) and Ra=10^9 (right).

tion of the magnetic field in the present turbulent flow cases is not that straightforward. In fact, as discussed in the next section, the cooling process during the next stage of stratification is decelerated by the magnetic field for the lower Rayleigh numbers studied and it is accelerated for the higher ones.

Figure 3 shows that near the bottom corner of the container, where the axial momentum of the vertical boundary layer is transferred to the radial direction, the intruding flow for Ha=300 is thicker than for the hydrodynamic case, which means that the presence of the magnetic field has the tendency to reduce faster the axial extent of the vertical boundary layer than in the hydrodynamic case. This probably happens because of the stronger magnetic damping of the flow in this region due to the higher radial velocities. Independently of the Rayleigh number, for $t>6$ the rising hydrodynamic flow reached the upper horizontal plate near the symmetry axis. The time needed for this rising becomes longer as the Hartmann number increases.

For $t=5$, the intrusion stage is almost finished, the axial and radial momentums are of the same magnitude, and the effect of the magnetic field is stronger even near the vertical boundary layer. As the fluid descends through it, the deceleration in the magnetohydrodynamic cases is proportional to the Hartmann number for the same Rayleigh number. However, the degree of influence of the magnetic field varies for different Rayleigh numbers as shown in Fig. 6 at $t=5$, for Ha=300 at Ra=10^7 and 10^9. The linear Lorentz force is less effective at higher Rayleigh number for the same Hartmann number. The radial distributions of temperature and axial velocity for the case of Ra=10^9 are very similar in the boundary layer for time $t=5$, while for the smaller Rayleigh number of 10^7 the results of the magnetohydrodynamic case differ. The flow in the boundary layer during the intrusion and stratification stages is decelerated due to the magnetic field action. Since the flow in the vertical boundary layer is mostly laminar, conduction heat transfer is promoted by the magnetic field.

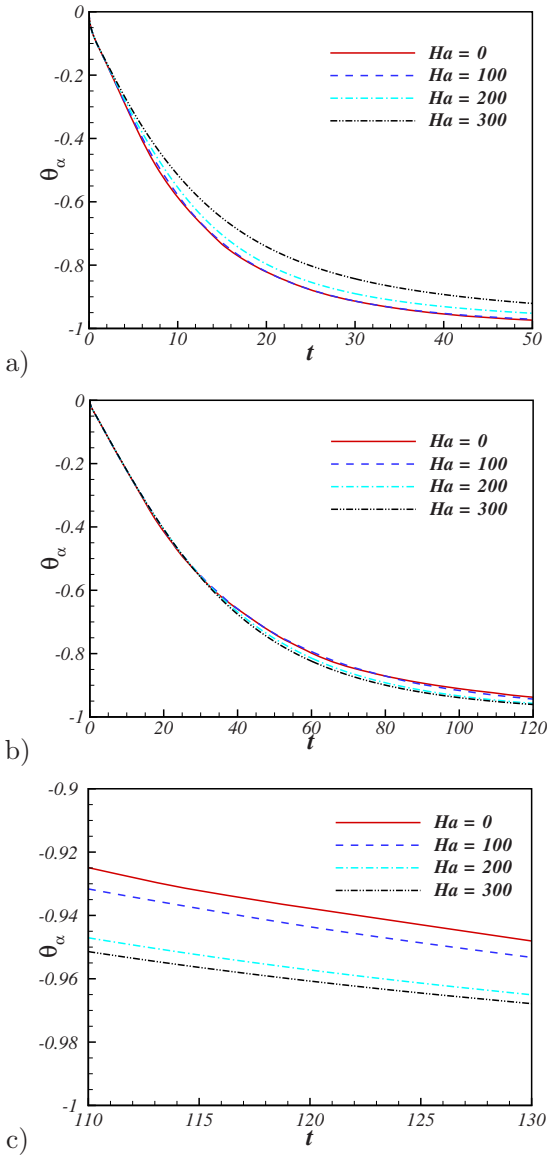

FIG. 7. (Color online) Time variation of the fluid average temperature, θ_α, for various Ha numbers: (a) Ra=10^7, (b) Ra=10^9, and (c) details of case (b) for $t>110$.

C. Flow stratification

After the intrusion stage and before the complete cooldown of the fluid, the stratification stage occurs. The cold fluid from the vertical boundary layer is mixed with the initially hot fluid of the bulk and progressively the average temperature in the container is becoming equal to that of the cold cylindrical wall. As shown in Fig. 7, the duration of the stratification stage depends on the value of the Rayleigh number. The average temperature reaches asymptotically an almost stationary value, higher than the temperature of the cold wall, and then the stratification stage finishes. The next stage of fluid cooldown is not discussed here because the magnetic field has a minor effect since the flow is rather slow during this asymptotic stage.

Figure 8 illustrates the different cooling mechanisms during the stratification stage for Ra=10^9 between the cases Ha=0 and 300. In the hydrodynamic case, the vortices that are produced in the lower corner of the container ascend and the cold fluid are transferred to the bulk. The cold fluid vortices are transferred both horizontally and vertically, resulting in a fully turbulent temperature distribution. In contrast, the magnetohydrodynamic stratification is fundamentally different. The fluid is injected from the same lower corner of the container but in larger vortices that travel mostly radially toward the axis. The fluid in the container is cooled progressively primarily by a turbulent motion and mixing in the radial/horizontal direction, in the region between the bottom wall and the stratification height and with minor fluctuations at the upper hot part of the stratified fluid. Small waves of cold fluid are formed close to the boundary layer that travels in the interface between the cold and the hot regions at the stratification height. These waves are produced by the dynamics of the cooling process and at short times (e.g., $t=10$) they exist in both cases of Ha=0 and 300. However, the suppression due to the magnetic field prevents the growth of these waves.

The existence of the traveling waves in the fluid is also

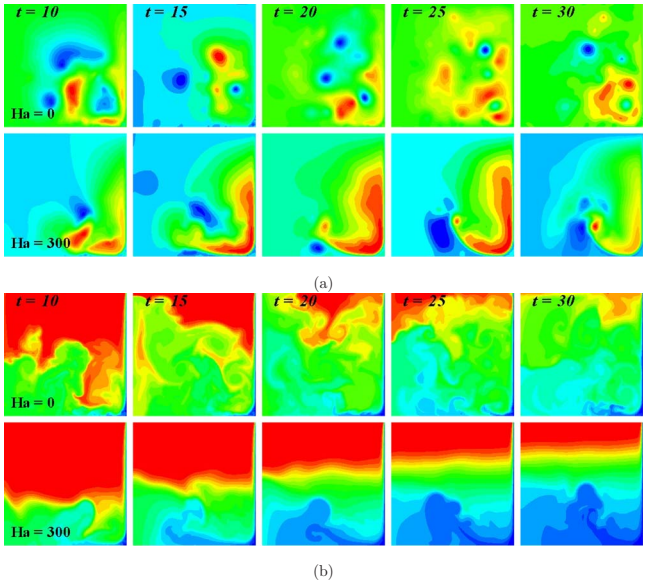

FIG. 8. (Color online) Streamfunction (a) and temperature fields (b) at $10 \leq t \leq 30$ for $Ra=10^9$: Ha=0 (upper) and Ha=300 (lower).

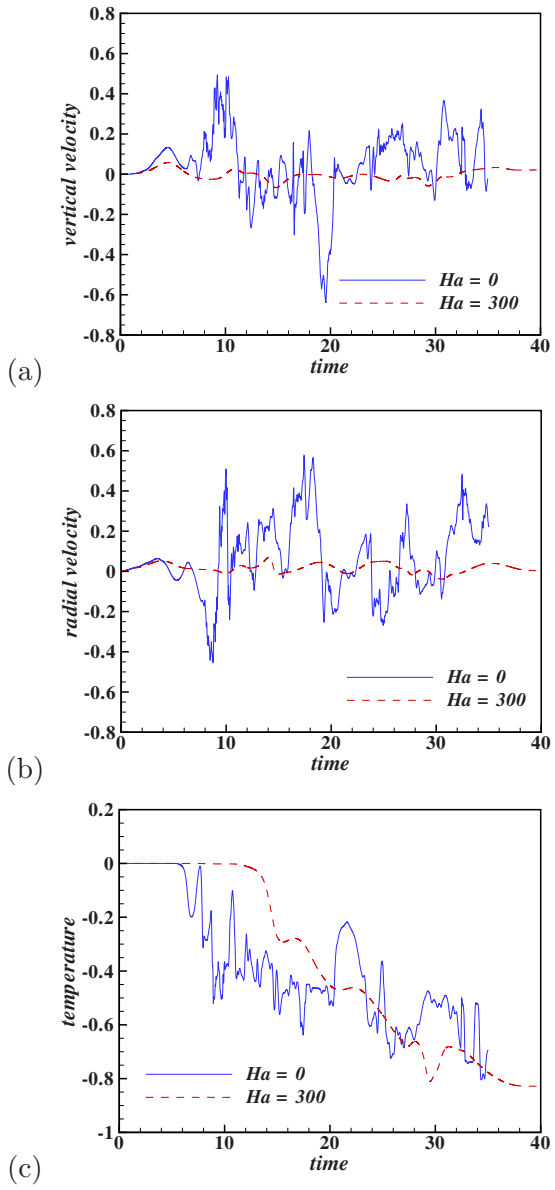

FIG. 9. (Color online) Time evolution of vertical velocity (a), radial velocity (b), and temperature (c) at position $r=0.5$, $z=0.5$ for $Ra=10^9$, Ha=0 and 300.

illustrated by the turbulent velocity bursts at the center of the computational domain shown in Fig. 9. This turbulent stratification was also shown without details, by Lin *et al.*[11] for their low-Pr fluid case, but no fluctuations are reported by Lin and Armfield[6] for the high-Pr regime. The turbulent fluctuations that are present in the hydrodynamic case are also observed for Ha=300, although smoother due to the magnetic damping. The increased fluid turbulence of the high-Ra case during the stratification stage is also apparent in the temperature variation shown in Fig. 9. The fluctuations of the temperature are initiated in the time period $5<t<10$ and are connected to the primary fluid bursts which ascend near the axis to the upper wall and descend through the vertical boundary layer to the bottom corner of the container. The evolution of the average fluid temperature after the intrusion bursts follows an exponential decay to the asymptotic cooldown, as shown in Fig. 7.

The average bulk temperature is a measure of the efficiency of fluid cooling during each stage. The increase in the magnetic field strength increases the time duration of the fluid cooldown, as shown in Fig. 7(a) for the low Rayleigh numbers. This result, however, is not true for the cases of higher Rayleigh numbers. As shown in Fig. 7(b) for the entire stratification stage and in Fig. 7(c) for longer times, the increasing magnetic field decreases the average bulk temperature. Thus, it appears that for high Rayleigh numbers the magnetic field accelerates the natural convection cooling, which is an interesting new finding.

This dependence of the effect of the magnetic field on the Rayleigh number during the stratification stage is rather unusual. The common understanding is that the Lorentz force has a damping effect, suggesting that the increase in the magnetic field should suppress the fluid motion, promote conduction heat transfer, and consequently delay the cooling process, like in the cases of low Rayleigh numbers. The observed reverse effect of the magnetic field for the high-Ra cases is due to the fundamentally different turbulent cooling mechanism. The horizontally traveling vortices in the magnetohydrodynamic cases are more effective in cooling the fluid than the vortices of the hydrodynamic case which are more in contact with the hotter bulk fluid. The consequence of the axial vortex motion is that hot fluid still remains in the bulk resulting in a reduction in the stratification rate. The translational speed of the horizontally moving vortices in the magnetohydrodynamic cases (and the associated cooling efficiency) is proportional to the local Rayleigh number. Thus, as the Hartmann number increases, the transient cooling during the stratification stage is promoted by the local temperature differences which may be higher in the boundary layer and in the interface with the hot fluid. In fact, the present flow is not the only case where the magnetic field enhances heat transfer. Heat transfer is also promoted in liquid metal

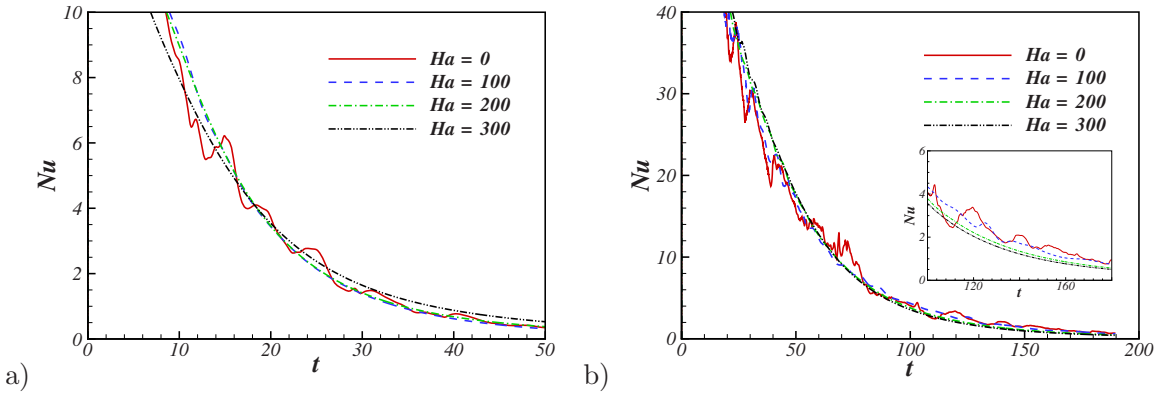

FIG. 10. (Color online) Temporal variation of the average Nu for different Ha: (a) Ra=10^7 and (b) Ra=10^9.

duct flows when high magnetic fields are applied, producing turbulent wakes in the side layers, Burr *et al.*[30]

The remaining horizontal motion of the vortices is also helped by the preservation of the vertical boundary layer in the magnetohydrodynamic cases. The extent of this boundary layer is becoming smaller with time and, in the hydrodynamic case, it collapses quicker. In contrast, for the magnetohydrodynamic cases, the boundary layer decreases without deforming. At time $t=20$, the stratification region of the magnetohydrodynamic case of Ra=10^9 and Ha=300 just passed the height $z=0.5$, as may be seen in Fig. 8(b). The variation in the momentum and thermal boundary layers at this instant may be assessed in Figs. 6(a) and 6(c) for Ra=10^7, and in Figs. 6(b) and 6(d) for Ra=10^9. This deformation is stronger in the case of the lower Rayleigh number. As the Rayleigh number increases, the deformation of the boundary layer is less extensive and in the magnetohydrodynamic case, the boundary layer is present during the entire stratification stage. The deceleration or acceleration of the cooling of the fluid due to the magnetic field for different Rayleigh numbers is also depicted in the calculated heat transfer at the vertical boundary, as indicated by the time evolution of the average Nusselt number shown in Fig. 10.

Finally, an additional result of the action of the magnetic field is also depicted in Fig. 8(b) after $t=25$. It is apparent from the isotherms that the magnetic field results in a strong local cooling action of the fluid in the vertical cylinder. In particular, two almost discrete regions of exclusively cold and hot fluid at the bottom and at the top area of the cylinder are formed, respectively, due to the action of the magnetic field. Thus, it appears that for the case of Ha=300 the bottom of the cylinder is cooled faster than the rest of the fluid or in the hydrodynamic case for the same Rayleigh number. The same effect of the magnetic field is observed for every Rayleigh number studied during the stratification stage. This technologically important feature is neither observed in the hydrodynamic case where the fluid due to the turbulent mixing is almost cooled uniformly nor when conduction is the dominant heat transfer mechanism. In the latter case, the cooling is expected to follow primarily the radial expansion and deformation of the vertical boundary layer.

IV. CONCLUSIONS

Direct numerical simulations were performed of the turbulent natural convection cooling of a hot low-Prandtl number fluid which was contained in a vertical cylinder in the presence of a constant vertical magnetic field. The analysis focused on the effect of the imposed magnetic field where it is expected that it will suppress the turbulent fluctuations, reduce the fluid motion, and consequently decelerate the natural convection cooling. It is observed that, in the initial stage of the development of the boundary layer on the cylindrical wall, there is no significant influence of the magnetic field. In the next stage of thermal intrusion of cold fluid, a significant reduction in heat transfer is observed in the presence of the magnetic field, while at the final stage of thermal stratification, the magnetic field decelerates the cooling of the low-Pr fluid for low Rayleigh numbers and accelerates it for high ones. This dependence of the magnetic field effect on the Rayleigh number is rather unusual and it was found to be related to the cold vortices emanating from the vertical boundary layer. The different cooling mechanism due to the magnetic field results in the fast local cooling of the bottom of the cylinder during the stratification stage. Finally, it should be repeated here that the present results were based on the assumption of axisymmetry, and the study of possible three-dimensional effects is proposed for future work.

ACKNOWLEDGMENTS

This work was performed in the framework of the EURATOM—Hellenic Republic Association and is supported by the European Union within the Fusion Program. The content of this publication is the sole responsibility of the authors and it does not necessarily represent the views of the Commission or its services.

[1]E. Papanicolaou and V. Belessiotis, "Transient natural convection in a cylindrical enclosure at high Rayleigh numbers," Int. J. Heat Mass Transfer **45**, 1425 (2002).
[2]S. H. Lee and J. M. Hyun, "Transient buoyant convection of air in an enclosure under strong magnetic effect," Int. J. Heat Mass Transfer **48**, 3097 (2005).

[3]L. Davoust, M. D. Cowley, R. Moreau, and R. Bolcato, "Buoyancy-driven convection with a uniform magnetic field. Part 2. Experimental investigation," J. Fluid Mech. **400**, 59 (1999).
[4]R. Verzicco and R. Camussi, "Numerical experiments on strongly turbulent thermal convection in a slender cylindrical cell," J. Fluid Mech. **477**, 19 (2003).
[5]I. E. Sarris, S. C. Kakarantzas, A. P. Grecos, and N. S. Vlachos, "MHD natural convection in a laterally and volumetrically heated square cavity," Int. J. Heat Mass Transfer **48**, 3443 (2005).
[6]W. Lin and S. W. Armfield, "Natural convection cooling of rectangular and cylindrical containers," Int. J. Heat Fluid Flow **22**, 72 (2001).
[7]J. M. Hyun, "Unsteady buoyancy convection in an enclosure," Adv. Heat Transfer **24**, 277 (1994).
[8]R. R. Nourgaliev, T. N. Dinh, and B. R. Sehgal, "Simulation and analysis of transient cooldown natural convection experiments," Nucl. Eng. Des. **178**, 13 (1997).
[9]J. M. Hyun, "Effect of the Prandtl number on heat-up of a stratified fluid in an enclosure," ASME Trans. J. Heat Transfer **107**, 982 (1985).
[10]W. Lin and S. W. Armfield, "Scaling laws for unsteady natural convection cooling of fluid with Prandtl number less than one in a vertical cylinder," Phys. Rev. E **72**, 016306 (2005).
[11]W. Lin, S. W. Armfield, and J. C. Patterson, "Cooling of a Pr<1 fluid in a rectangular container," J. Fluid Mech. **574**, 85 (2007).
[12]B. Knaepen and P. Moin, "Large-eddy simulation of conductive flows at low magnetic Reynolds number," Phys. Fluids **16**, 1255 (2004).
[13]S. Kenjereš and K. Hanjalić, "On the implementation of effects of Lorentz force in turbulence closure models," Int. J. Heat Fluid Flow **21**, 329 (2000).
[14]R. M. Kerr and J. R. Herring, "Prandtl number dependence of Nusselt number in direct numerical simulations," J. Fluid Mech. **419**, 325 (2000).
[15]R. Moreau, *Magnetohydrodynamics* (Kluwer Academic, London, 1998).
[16]I. E. Sarris, G. K. Zikos, A. P. Grecos, and N. S. Vlachos, "On the limits of validity of the low magnetic Reynolds number approximation in MHD natural convection heat transfer," Numerical Heat Transfer, Part B **50**, 157 (2006).
[17]S. C. Kakarantzas, I. E. Sarris, A. P. Grecos, and N. S. Vlachos, "Magnetohydrodynamic natural convection in a sinusoidal upper heated cylindrical cavity," Int. J. Heat Mass Transfer **52**, 250 (2009).
[18]B. Knaepen and R. Moreau, "Magnetohydrodynamic turbulence at low magnetic Reynolds number," Annu. Rev. Fluid Mech. **40**, 25 (2008).
[19]S. C. Kakarantzas, A. P. Grecos, N. S. Vlachos, I. E. Sarris, B. Knaepen, and D. Carati, "Direct numerical simulation of a heat removal configuration for fusion blankets," Energy Convers. Manage. **48**, 2775 (2007).
[20]A. Yu. Gelfgat and P. Z. Bar-Yoseph, "The effect of an external magnetic field on oscillatory instability of convective flows in a rectangular cavity," Phys. Fluids **13**, 2269 (2001).
[21]R. Verzicco and P. Orlandi, "A finite-difference scheme for three-dimensional incompressible flow in cylindrical coordinates," J. Comput. Phys. **123**, 402 (1996).
[22]P. Orlandi, *Fluid Flow Phenomena: A Numerical Toolkit* (Kluwer Academic, London, 2001).
[23]P. Swarztrauber and R. Sweet, "Efficient FORTRAN subprograms for the solution of elliptic partial differential equations," NCAR Technical Report No. TN/IA-109, 1975.
[24]T. Alboussière and R. J. Lingwood, "A model for the turbulent Hartmann layer," Phys. Fluids **12**, 1535 (2000).
[25]W. Lin and S. W. Armfield, "Direct simulation of natural convection cooling in a vertical circular cylinder," Int. J. Heat Mass Transfer **42**, 4117 (1999).
[26]G. Grötzbach, "Spatial resolution requirements for direct numerical simulation of the Rayleigh–Bernard convection," J. Comput. Phys. **49**, 241 (1983).
[27]P. Moin and K. Mahesh, "Direct numerical simulation: A tool in turbulence research," Annu. Rev. Fluid Mech. **30**, 539 (1998).
[28]J. M. Aurnou and P. L. Olson, "Experiments on Rayleigh–Bernard convection, magnetoconvection and rotating magnetoconvection in liquid gallium," J. Fluid Mech. **430**, 283 (2001).
[29]W. Lin and S. W. Armfield, "Long-term behavior of cooling fluid in a vertical cylinder," Int. J. Heat Mass Transfer **48**, 53 (2005).
[30]U. Burr, L. Barleon, U. Muller, and A. Tsinober, "Turbulent transport of momentum and heat in magnetohydrodynamic rectangular duct flow with strong sidewall jets," J. Fluid Mech. **406**, 247 (2000).